



OPEN ACCESS

EDITED BY

Hao Shi,
Anhui University of Science and Technology,
China

REVIEWED BY

Pei Guo,
National Institute of Clean and Low-Carbon
Energy, China
Nao Lv,
Anhui University of Science and Technology,
China

*CORRESPONDENCE

Ling Zhang,
✉ cstzhangling@163.com

RECEIVED 18 April 2024

ACCEPTED 14 May 2024

PUBLISHED 05 June 2024

CITATION

Zhang Q, Zhang L and Jiang X (2024),
Acoustic emission characteristics and fracture
mechanism of sandstone in open-pit mines
under different types of cyclic loads.
Front. Earth Sci. 12:1419604.
doi: 10.3389/feart.2024.1419604

COPYRIGHT

© 2024 Zhang, Zhang and Jiang. This is an
open-access article distributed under the
terms of the [Creative Commons Attribution
License \(CC BY\)](https://creativecommons.org/licenses/by/4.0/). The use, distribution or
reproduction in other forums is permitted,
provided the original author(s) and the
copyright owner(s) are credited and that the
original publication in this journal is cited, in
accordance with accepted academic practice.
No use, distribution or reproduction is
permitted which does not comply with these
terms.

Acoustic emission characteristics and fracture mechanism of sandstone in open-pit mines under different types of cyclic loads

Qing Zhang¹, Ling Zhang^{2*} and Xutong Jiang²

¹College of Safety Science and Engineering, Xi'an University of Science and Technology, Xi'an, China,

²Cathay Safety Technology Co., Ltd., Beijing, China

Rock mass is one of the most important load-bearing media in geotechnical engineering. It has been continually vulnerable to geological tectonic movements, natural calamities, and human excavation activities. Its inherent weak surfaces such as primary pores, joints, and fissures have resulted in varying damage degrees. In mining operations, the damaged rock mass has a variety of negative impacts on the stability of its overlying structures and is frequently disturbed by the load. To study the damage law of rock mass under cyclic loading, in this paper, an acoustic emission (AE) device was employed to monitor the rock under the action of two types of cyclic loads: the variable upper and lower pre-loads, and the fixed upper and lower pre-loads. The damage of the loaded rock was split into three stages in this research, based on the features of the AE signals of the rock under uniaxial load, and the damage evolution of the loaded rock was analyzed in distinct stages. The AE signals of the rock under cyclic loading were mainly emitted in the first loading stage. When the stress did not exceed the maximum stress value in the stress history of the loaded rock, few new AE event was generated in the loaded rock. After the low-frequency cyclic static load, the AE signals varied with the load-bearing stress of the rock during the whole process from initial loading to failure, which was consistent with the characteristics of the AE signals of the loaded rock. The research results can be adapted to rock mass in open-pit mines stability analysis and risk prediction while providing some references for the early warning and danger relief of rock masses in engineering.

KEYWORDS

acoustic emission, cyclic loading, damage rock, rock mechanics, fracture mode

1 Introduction

Rock mass in geotechnical engineering is not only affected by original pores (Liu X. S. et al., 2016; Zheng et al., 2024), joints (Shi et al., 2023a; Shi et al., 2023b), and fissures (Si et al., 2024), but also by geological tectonic movement (Qian et al., 2018a), natural disasters (Li N. et al., 2020; Wu et al., 2020), and human mining activities (Zheng et al., 2020). Although the load applied on the rock mass is not necessarily the same each time, usually, the rock mass is affected by the external load more than once (Song et al., 2020; Xin et al., 2021), such as close coal seam mining (Tan et al., 2010; Qian et al., 2022),

double-arch tunnel construction (Luo et al., 2020), and so forth (Liu et al., 2020). The cyclic loads applied to the rock cause its interior in distinct degrees of damage state (Liu et al., 2016b), which have a negative effect on the mechanical properties of the rock mass (Ferrero et al., 2010; Zhu et al., 2022). It has the potential to induce the rock mass to lose its bearing capability, posing a significant hidden threat to the national economy and personal safety (Zheng et al., 2021a). Engineers and scientists place a high value on the research of rock damage under cyclic stress, which is critical for geotechnical engineering safety design and stability evaluation (Vaneghi et al., 2018; Chen W. et al., 2020).

Under the application of cyclic loading, the internal structure of the rock deteriorates to varying damage degrees, including the avianize of original flaws and the creation and propagation of cracks (Wu et al., 2020; Liu et al., 2021). These processes are accompanied by the deterioration of the microstructure of the rock (Wang et al., 2018), the reduction of macroscopic strength (Qian et al., 2018b), and energy dissipation (Marinelli et al., 2018). Due to the rock being a continuous opaque bearing medium, the structural state and damage in the rock under the load cannot be directly observed (Waples et al., 2004). Many scholars have extensively studied the strength change, deformation characteristics, and fracture mechanism of rocks under cyclic loading by means of numerical simulation (Borodii et al., 2010; Wei et al., 2020). However, the occurrence conditions and bearing characteristics of the rock mass are being simplified by the numerical simulation, and it is somewhat different between the calculated results and the actual engineering. In addition, some scholars adopt CT scanning to perform CT imaging of the loading process of the bearing rock (Ma et al., 2014; Sun et al., 2016). Nonetheless, the experimental results are limited by the accuracy of the operators, the expensive test, and the poor adaptability of the project site.

As the load on the rock grows, the internal cracks develop, extend, and penetrate, while wave signals that could be detected by sensors and carry a wealth of mechanical features of the rock are emitted (Yang et al., 2011; Zheng et al., 2021b). An in-depth analysis of these wave signals is necessary to study the mechanism of rock damage and fracture. The AE technology works on the basis of detecting the elastic wave released inside the rock during the loading process to monitor the test specimen constantly and in real-time (Liu et al., 2015; Zheng et al., 2019). The damage degree and fracture mechanism of the rock are investigated by studying the waveform signals emitted during the loading process (Li et al., 2016; Li Q. et al., 2020). This method of real-time monitoring of the loaded rock mass is closer to the actual project and has a wide range of applications, which can be applied to outdoor large-scale rock engineering.

The mechanical characteristics of rock mass under cyclic loading are related to the occurrence environment, bearing state, cycle times, and lithology (Kan et al., 2021; Li et al., 2021). Under the application of high-frequency cycle loads, the mechanical characteristics of rocks have been extensively studied, which not only enriches the rock mechanical theory, but also successfully guarantees engineering safety (Liu et al., 2020; Ghasemi et al., 2021). That notwithstanding, most of the maximum stress of the bearing rock mass in engineering is less than 80% of its bearing limit (Khaledi et al., 2016; Song et al., 2019). While the applied load is greater than 80% of its strength limit, the density of cracks in the rock is relatively high and the main crack

has already formed an embryonic shape (Yang et al., 2022). At this time, the mechanical characteristics of rock mass change due to the variety of its internal structure (Zheng et al., 2021b). Furthermore, after the stress exceeded 80% of the bearing limit, the mechanical characteristics of the rock mass changed rapidly and could not be correctly characterized numerically. Therefore, the mechanical characteristics and AE response laws of rocks under low-frequency cyclic loading are studied in this article only.

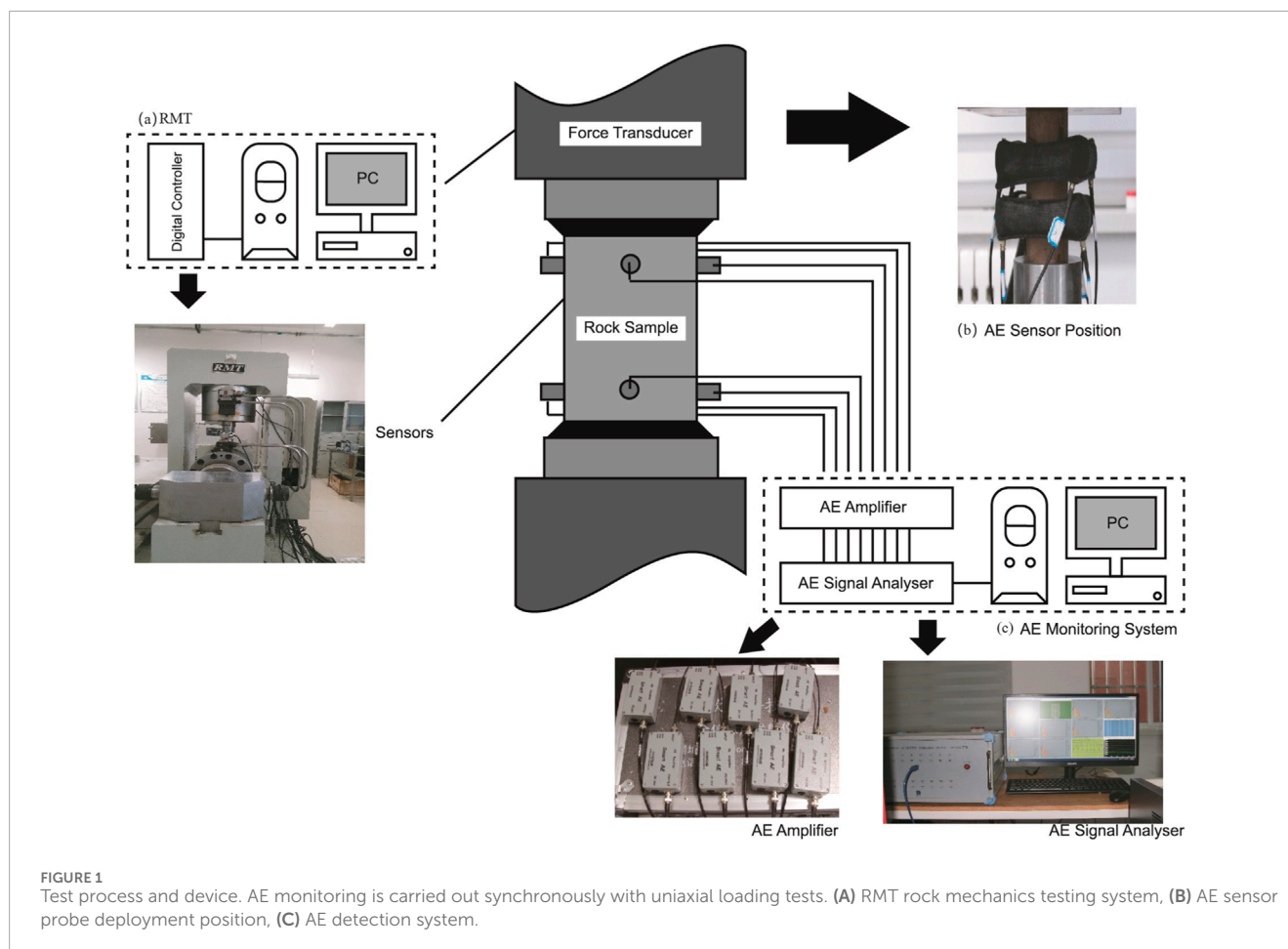
In this paper, the cyclic loading was employed to apply to the rock, and the characteristics of the AE signals about the rock under the cyclic load were studied. Firstly, the characteristics of AE signals and fracture mechanism of rock under uniaxial load were studied. In the meanwhile, the uniaxial compressive strength of the rock was measured. Then, took the uniaxial compressive strength of the rock as a reference, cyclic loads with diverse pre-loads were applied to the rock, and the AE signals characteristics of the rock under the application of different cyclic loads were studied. Finally, the cyclic load with the fixed pre-load was applied to the rock, and the relationship between the characteristics of the AE signals about the rock under the cyclic load was studied more comprehensively. The research results can be used to the stability and risk prediction of rock mass, at the same time, provide some references to the early warning and danger relief of rock mass in engineering.

2 Experiment

In this study, the sandstone selected was cored from an open-pit mine in China adopting *in-situ* sampling as the research object. In the light of the standards specified by the International Society for Rock Mechanics, a standard cylindrical rock with a size of Φ 50 mm \times h 100 mm was prepared. Of paramount importance is the mitigation of stress concentration on the sandstone during the loading procedure to ensure the precision of test outcomes. This was achieved by maintaining a flatness tolerance of both ends at less than 0.02 mm and ensuring a vertical error between the axis and the end faces of less than 0.001 rad. In addition, the sample of cyclic loading and unloading experiment also adopted this size.

The Rock Mechanics Test System (RMT-150B) was employed to test the strength of the sandstone and the cyclic loading as the loading system. The DS-5 AE device made in Ruandao Co. Ltd., which could store the AE parameters, was employed to monitor the loaded rock. In this experiment, eight sensors were employed for each rock to monitor and save AE signal parameters. The test process and device are shown in Figure 1.

For the sake of enhancing the monitoring effect, Vaseline was uniformly applied to the rock of the pre-designed location to receive signals. To reduce errors caused by AE sensor deviations, the placement of sensors must be the same for different sandstone specimens. Sensors 1-4 are uniformly arranged in a clockwise manner at a distance of 15 mm from the upper-end face of the rock, while sensors 5-8 are also uniformly arranged in a clockwise manner at a distance of 15 mm from the lower-end face of the rock, and sensors one and five are along the same axis. At the start of the experiment, a lead-breaking test was carried out with a pencil lead as a simulated source to calibrate the positioning test of the AE source and the sound velocity measurement test, and at the same time to determine the sensitivity of the ceramic probe to the AE



source. Moreover, interference from irrelevant sound sources such as collisions and frictions other than the loaded rock to be measured should be eliminated, and the monitoring should be started after the equipment was measured accurately. The acoustic emission and RMT work synchronously to complete the loading and monitoring test. The RMT applied load to the sandstone at an axial loading rate of 0.5 kN/s, and stored the mechanical test parameters in real-time. The AE monitoring system processed and stored the waveform signals monitored by the eight sensors, and obtained the waveform parameters of the sandstone under uniaxial load and the AE source location.

The cyclic loading experiment was based on the uniaxial compressive strength of the sandstone tested by the static mechanic's experiment was recorded as σ_b . Then, the sandstones were subjected to cyclic loading with different stress thresholds to make them in distinct damage degrees. The pre-load was $0.2 \sigma_b$, $0.4 \sigma_b$, $0.6 \sigma_b$, and $0.8 \sigma_b$, respectively, and the number of cycles of cyclic loading-unloading was 7. When the pre-load is $0.8 \sigma_b$, the size and number of cracks inside the sandstone are relatively large, but the integrity of the standard sample is still maintained on the outside of the rock sample. It should be noted that under the action of low stress, the oil pressure of the loading system may be unstable during the loading-unloading process, which affects the accuracy of the experimental results. Therefore, apart from the lower stress limit is 0 when the pre-load is $0.2 \sigma_b$, the lower pre-load of the rock under the cyclic

load of the remaining stress thresholds is $0.2 \sigma_b$. On the one hand, the error caused by the instability of the oil pressure of the loading system under the action of low stress was avoided; on the other hand, the cyclic loading and unloading test with a pre-load of $0.2 \sigma_b$ was also within the scope of this experiment. Combined with the control group, the mechanical properties of rocks under cyclic loading with different stress thresholds could be directly studied. The layout of the AE monitoring system was consistent with that of the uniaxial loading test.

3 Results and discussions

3.1 Uniaxial compressive strength of sandstone

On the basis of the test results, as shown in [Table 1](#), the rocks' strength is summary. According to the uniaxial compressive test results of sandstone, the average strength $\bar{\sigma}_b$ is 62.68 MPa.

Combined with the rock mechanics theory, the loading process could be divided into four stages: original micro-pores were compacted and closed, elastic deformation stage, crack propagation stage, and the residual strength stage. The extent of damage at different stages was closely related to its internal structure and fracture mode. Thus, before studying the damage of the sandstone,

TABLE 1 Strength table of sandstone.

| Number | σ_b (MPa) | ε (%) |
|-------------------------------------|------------------|-------------------|
| S-1 | 59.28 | 0.781 |
| S-2 | 58.35 | 0.773 |
| S-3 | 66.36 | 0.896 |
| S-4 | 63.15 | 0.802 |
| S-5 | 66.28 | 0.912 |
| $\bar{\sigma}_b$ (Average strength) | 62.68 | 0.833 |

it was necessary to shed light on the four stages of its mechanical characteristics in conjunction with the changes in the internal structure. The sandstone's physical characteristics and diagenetic environment determined how the fissures were squeezed and closed in the previous four stages. As a result of the loading, the sandstone's inherent micropores were gradually squeezed and closed. The solid mineral particles inside the rock performed a crucial role in resisting deformation when the load rose after the original micro-pores were closed. The deformation of the rock could be recovered with the removal of the load from now to the stage before the crack propagation, and the loaded rock was in the elastic deformation stage. Once the elastic period is through, the fractures in the rock begin to expand rapidly. As a result of the crack tip effect, the cracks expanded in size and caused secondary cracks, which in turn induced further cracks on a repeating basis. The number of fissures in the rock multiplied exponentially until the primary crack pierced the rock and lost bearing capacity. The appearance of the macroscopic mechanical features of the sandstone superficies was the result of the qualitative change caused by the quantitative change of the internal micromechanics of the sandstone under the load. As a result, the mechanical properties and failure process could be better understood by studying the changes in the meso-mechanical features of the sandstone under stress. These meso-mechanical features of sandstones under load could be obtained by real-time monitoring by AE in the form of waveform signals. Then, the sandstone AE parameters were studied to characterize the mechanical properties and fracture mechanism.

3.2 AE characteristics of loaded sandstone

The AE signal parameters AE energy, cumulative count, average frequency (AF), and rising angle (RA) provide an abundance of rock mechanics information, including the rock's deterioration and fracture mechanism. The relationship between the time-stress-AE energy-accumulative count of AE events of the loaded sandstone was obtained by investigating the AE signals monitored during the uniaxial compression test of the sandstone, as shown in Figure 2, and the mechanical properties and fracture mechanism of the sandstone were studied. The AE signal of sandstone under load was classified into three phases based on the features of the AE signal curve:

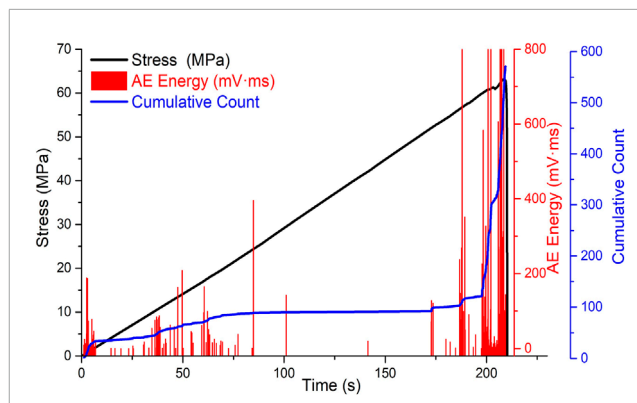


FIGURE 2 Relationship between the four parameters of the loaded sandstone AE signals. The characteristics of AE signals are divided into three stages: rapid increase in a short period first, then relatively gentle and with few events, and finally, rapid increase in a short period before destruction.

initially-emitting phase, stably-emitting phase, and rapidly-emitting phase.

According to the AE signals features of sandstone, in the three phases of the AE signals features of the same loaded sandstone, the cumulative count per second, denoted as $\Delta HR/\Delta t$, achieved the maximum in the second half of the rapidly-emitting phase, as shown in Table 2, and the minimum during the stably-emitting phase. The AE energy achieved the maximum in the second half of the rapidly-emitting phase, and was the smallest in the initially-emitting phase.

The AE events were predominantly emitted by the compaction and closure of the original micro-pores in the sandstone during the initially-emitting phase, that is, when the original micro-pores of the sandstone were compressed and closed. When the main pores were compressed and closed, the elastic wave energy was low, and the intensity of AE events was low compared to the other stages. As a result, the AE events in the loaded sandstone were intense at this phase, as shown in Figure 2. The $\Delta HR/\Delta t$ value was relatively big, although the AE energy was not less than $300 \text{ mV} \cdot \text{ms}$. When the bigger original micro-pores in the loaded sandstone were compressed and closed, the AE energy was more than the value of the smaller original micro-pores. Among a great deal of planes along the length direction, the fissures of the plane species with higher pore density were more compacted and closed. In this stage, the AE signal features of the loaded sandstone were low energy and large $\Delta HR/\Delta t$. The AE energy of the loaded sandstone, on the contrary, was high, and the $\Delta HR/\Delta t$ was low, as indicated in Figure 2; Table 2.

The loading sandstone attained the elastic deformation stage as the load increased. The elastic deformation of gravels dominated the rock's deformation at this time, which was accompanied by the compacting and sealing of a small number of initial micro-pores, as well as the commencement of cracks in the local area. Meanwhile, as shown in Figure 2; Table 2, the loaded rock's AE signals had the following features: the AE energy was relatively low but greater than the value in the initially-emitting phase, and the $\Delta HR/\Delta t$ was the smallest. There was still a tiny portion of the original micro-pores that was not entirely compressed and closed during the initial elastic

TABLE 2 Parameter characteristic table of different AE signal phases for different sandstones.

| Number | Characteristic phase of AE signals | $\Delta HR/\Delta t$ |
|--------|------------------------------------|----------------------|
| S-1 | Initially-emitting phase | 2.86560 |
| | Stably-emitting phase | 0.17946 |
| | Rapidly-emitting phase | 8.33105 |
| S-2 | Initially-emitting phase | 1.91757 |
| | Stably-emitting phase | 0.22848 |
| | Rapidly-emitting phase | 8.24857 |
| S-3 | Initially-emitting phase | 2.00411 |
| | Stably-emitting phase | 0.09445 |
| | Rapidly-emitting phase | 4.70390 |
| S-4 | Initially-emitting phase | 4.94678 |
| | Stably-emitting phase | 0.47567 |
| | Rapidly-emitting phase | 37.8721 |
| S-5 | Initially-emitting phase | 5.19443 |
| | Stably-emitting phase | 0.00563 |
| | Rapidly-emitting phase | 6.37852 |

deformation stage. When the solid mineral particles flex elastically until their size was too small to oppose the closed size of the original micro-pores, the original micro-pores began to close and emit AE events in the same plane along the height of the sandstone. As a result, all original micro-pores in the loaded sandstone's initial stage were not entirely closed. Some original micro-pores were compressed and closed during the elastic deformation stage, particularly in the early stages, but the number was modest and not intensity. The deformation of the loaded sandstone during the elastic deformation stage was mostly due to the deformation of the solid mineral particles. The elastic deformation of the gravels under the application of the load steadily increased as the load rose. From a microscopic perspective, the gravels and the cementitious matrix might be considered an element when they resisted the force, and the rock was made up of numerous such elements. Meanwhile, the rock's interior structure remained reasonably stable, the number of AE events was low, and the AE energy was low. The transition surface between the gravels and the cemented matrix would begin fractures under stress as the load increased, emitting AE signals. As the load was increased, the cracks formed during the compacting and closure phase of the initial fractures, as well as the cracks formed during the elastic stage by the tension between the gravels and the cemented matrix, grew owing to the stress concentration at the crack tip. The loaded rock is now at the crack propagation stage.

The loaded sandstone entered the rapidly-emitting phase after cracks in various spaces within the sandstone began to grow rapidly

with the application of the load, the cracks propagation induced secondary cracks, which gradually extended under the influence of the crack tip effect, and the cracked sandstone entered the rapidly-emitting phase. As demonstrated in Figure 2; Table 2, the values of AE energy and $\Delta HR/\Delta t$ both achieved their maximums in comparison to the preceding two stages. In the elastic stage, the enlarged area of the contact surface between the gravels and the cemented matrix was larger and quicker than the area of crack propagation in the loaded sandstone. As a result, the AE signal emitted was more intense, and the AE energy was likewise higher. Secondary cracks developed as the original fractures expanded, and the number of fissures in the loaded rock increased exponentially. As a result, $\Delta HR/\Delta t$ had the highest value. The pace of fracture propagation increased as the load rose until the primary crack pierced the sandstone and became unstable. The AE energy and $\Delta HR/\Delta t$ both achieved their maximums before the main crack extended till the major crack penetrated.

The observed AE events were identified, as indicated in Figure 3, to validate the features of AE signals of sandstone under uniaxial force. It was possible to determine that the quantity and intensity of AE events in the loaded sandstone changed as stress increased by identifying AE events in the loaded sandstone. The AE event emitted from the loaded rock at the initially-emitting phase of loading, which was primarily produced by the compaction and closure of the major pores, as evidenced by the AE event location of the loaded rock. The elastic deformation of the gravels against the load produced the deformation of the loaded rock in the elastic deformation stage, and it could be recovered once the external force was withdrawn. As a result, there were fewer AE events during this stage. The interior fissures began to grow and produce secondary fractures while the loaded rock was in the plastic deformation stage, until the rock lost stability. The AE events generated by the loaded sandstone were the most powerful at this moment. This outcome was similarly identical to the one shown in Figure 2.

The mechanical properties and damage laws of the loaded sandstone were examined by evaluating the AE signal parameters of the loaded sandstone. In reality, in geotechnical engineering, the stress on the rock mass was generally reciprocating. As a result, studying the mechanical features and AE signal features of the sandstone under uniaxial stress was insufficient to completely comprehend the damage characteristics and load-bearing laws of rock masses in geotechnical engineering. On the basis of the sandstone damage law and AE signal characteristics under uniaxial load analyzed above, this paper adopts different cyclic static load stress upper limits to apply to sandstone to study the rock damage and AE signal response law under low-frequency cyclic loading.

3.3 AE signal characteristics of sandstone under cyclic load

For the sake of better comprehensively grasping the AE signal characteristics of rocks under cyclic loading. In this paper, two methods of setting variable upper and lower limits, and the fixed upper and lower limits were used to carry out cyclic loading and unloading tests on rocks to study the mechanical properties and AE signal characteristics of rocks under different cyclic loading and unloading. In addition, the experimental results of the cyclic

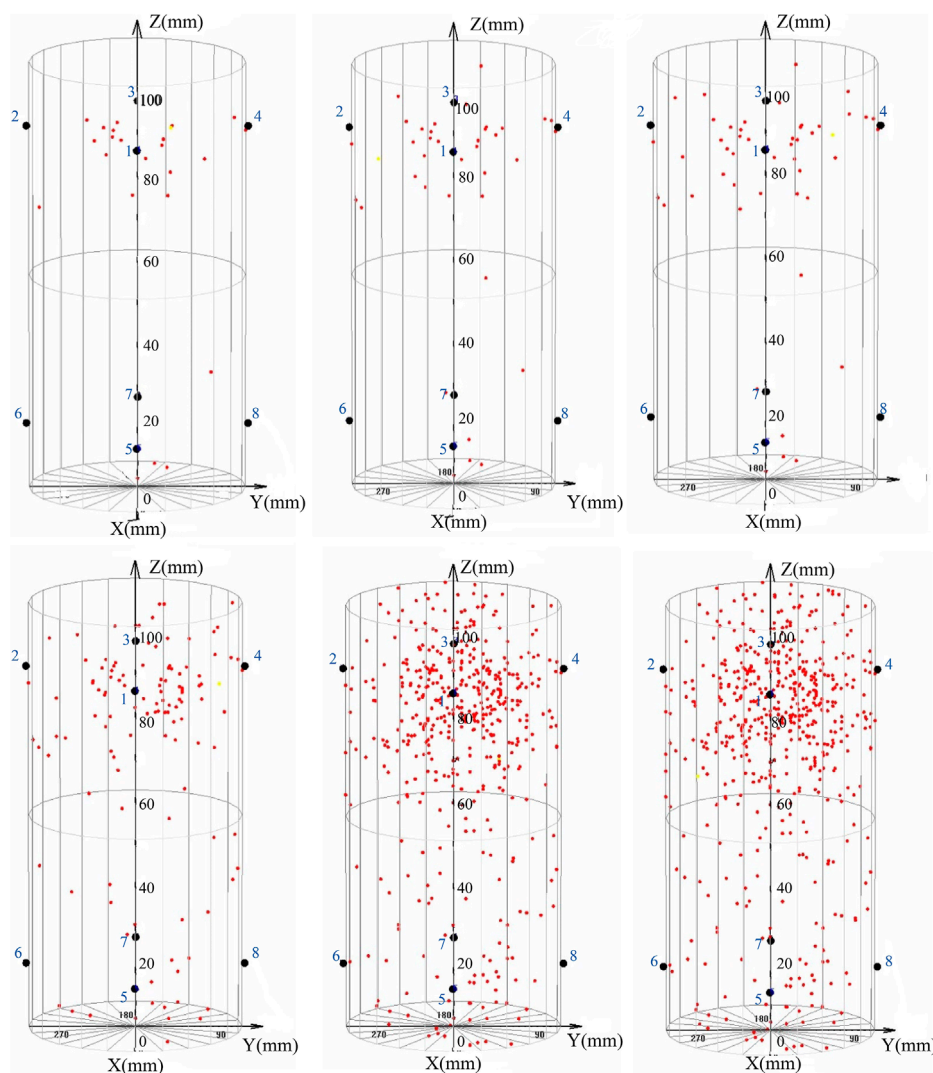


FIGURE 3

Location of AE events in the loaded rock. The number of AE events increases with the load rising, and the growth pattern also conforms to the AE signal characteristic curve in Figure 2. The blue numbers in the figure represent the position of the sensor probes, and the red dots are the position of the AE events.

loading were verified by continuing the loading until the failure and instability after the cyclic loading.

First, analyzed the characteristics of AE signal of rock under the action of cyclic load with fixed upper and lower limits. In the light of the uniaxial compressive strength σ_b of the rock measured under the uniaxial load, the sandstones were subjected to cyclic loading and unloading tests with different cyclic threshold loads to make them in different damage states. The cycle threshold load was $0.2 \sigma_b$, $0.4 \sigma_b$, $0.6 \sigma_b$, and $0.8 \sigma_b$, respectively, and the number of cycles of loading and unloading was 7. In order to prevent the error caused by the unstable oil pressure of the pressure system under low stress, excepted for the lower stress limit of 0 when the upper limit of the cyclic static load stress was $0.2 \sigma_b$, the lower stress limit corresponding to the other upper-stress limits were all $0.2 \sigma_b$. For the AE signal characteristics of the rock under cyclic loading when it was less than $0.2 \sigma_b$, it could be analyzed from the situation that the

upper limit of the cyclic static load stress was $0.2 \sigma_b$. Figure 4 shows the characteristics of AE signal of rock under different upper-stress limit cyclic loading.

It can be seen from the experimental results in Figure 4 that the rock is subjected to cyclic loads with different upper-stress limits. Excepted for the obvious AE events in the first loading and unloading stage, the proportion of AE events in the subsequent six stages was very small. In the first loading and unloading stage of sandstone, when the upper-stress limit was $0.2 \sigma_b$, $0.4 \sigma_b$, $0.6 \sigma_b$, and $0.8 \sigma_b$, the number of AE events accounted for 83.33%, 94.12%, 85.13%, and 88.41% of the total number of AE events in the entire experiment. Among them, the proportions of the loading stage in the first loading and unloading stage were 79.56%, 93.58%, 84.10%, and 84.78%, successively. It could be seen that in the entire process of cyclic loading and unloading, the first loading stage accounted for the largest proportion. It could be

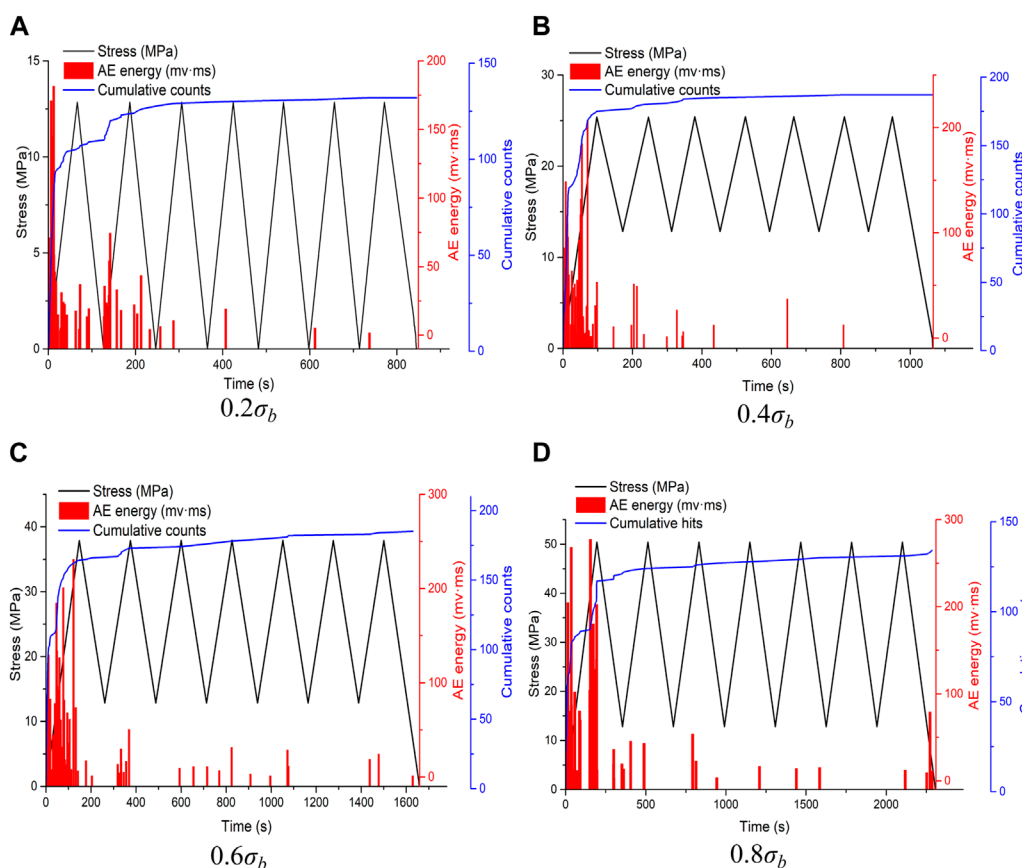


FIGURE 4 AE signal characteristics of rock under fixed upper and lower limit cyclic loading. AE events are mainly concentrated in the first loading stage and are almost rare after the completion of the first loading stage. (A) $0.2\sigma_b$, (B) $0.4\sigma_b$, (C) $0.6\sigma_b$, and (D) $0.8\sigma_b$.

seen from Figure 4 that compared with the other three upper-stress conditions, when the upper-stress limit was $0.2\sigma_b$, the proportion of AE events in the remaining test stages except the first loading stage was the largest. It was because of the error caused by the unstable oil pressure of the experimental device under low-stress cyclic loading. Therefore, when the upper-stress limit of the cyclic static load stress was greater than $0.2\sigma_b$, the lower-stress limit of the cyclic loading and unloading test was $0.2\sigma_b$, and for the characteristics of the AE signal when the stress was lower than $0.2\sigma_b$, please refer to the cyclic loading and unloading test when the upper-stress limit was $0.2\sigma_b$. Figure 4 illustrates the AE signal characteristics of sandstones subjected to varying upper-limit static loads. It demonstrates that in sandstone, under static loads not exceeding the maximum value in stress history, few new AE events occur. However, a loading method with a fixed lower limit and a variable upper limit was used to indicate that with increasing upper-limit static loads, there is a corresponding increase in AE events.

In order to analyze the AE signal characteristics of the rock under cyclic loading with different upper-stress limits more intuitively, a loading method with a fixed lower limit and a variable upper limit was used to analyze the AE signal characteristics of the rock under the cyclic load. The lower-stress limit was 0, and the upper-stress limit was $0.2\sigma_b$, $0.4\sigma_b$, $0.6\sigma_b$, and

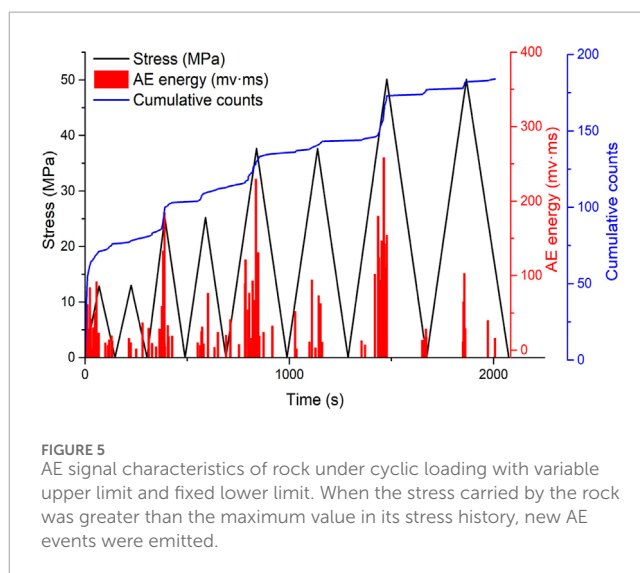
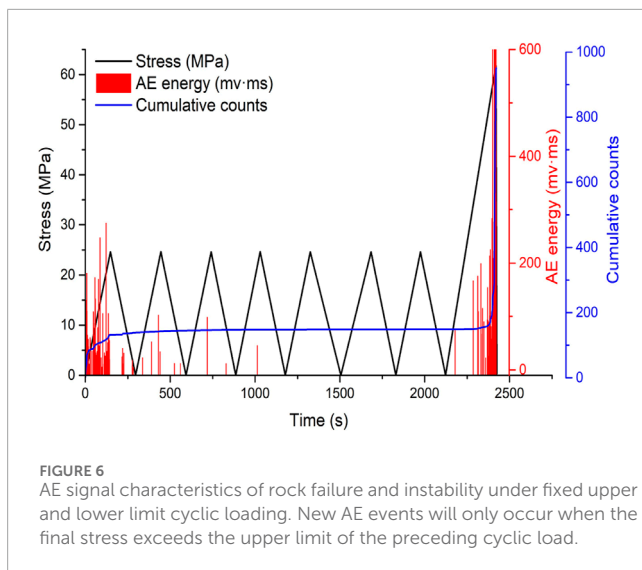


FIGURE 5 AE signal characteristics of rock under cyclic loading with variable upper limit and fixed lower limit. When the stress carried by the rock was greater than the maximum value in its stress history, new AE events were emitted.

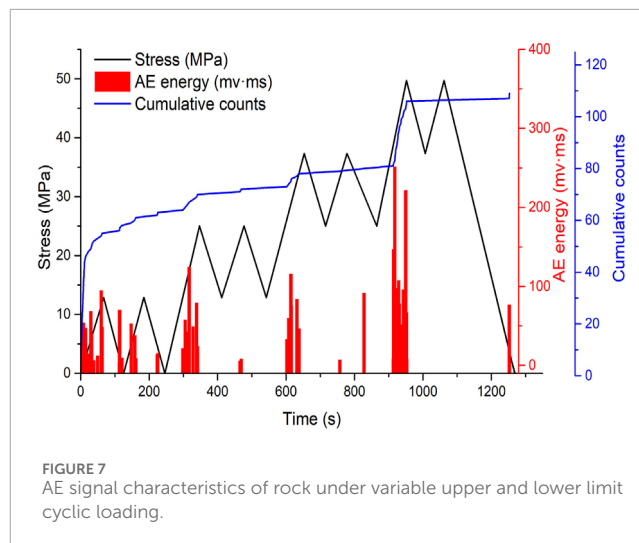
$0.8\sigma_b$, respectively and increased in sequence. The number of cycles of each upper-stress limit was 2 times, as shown in Figure 5.



The experimental results in Figure 5 further verified the AE signal characteristics of the rock under the action of cyclic loads with different upper-stress limits in Figure 4. Within the cyclic loading and unloading range of the same magnitude of upper-stress limit, the AE event mainly occurred in the loading phase of the first loading and unloading stage, and there were fewer AE events in the other stages within the range of this stage. When the bearing stress of the loaded rock was not greater than the maximum stress of the previous stage, there were few AE events in the loaded sandstone. As shown in the areas a, b, and c in Figure 5, within the range of the initial loading stage of each upper-stress limit, when the rock was at a stress level not greater than the previous upper-stress limit, there were almost no or very few AE events in the loaded rock. When the stress carried by the rock was greater than the maximum value in its stress history, a new AE event was emitted. This result was consistent with the test result in Figure 4.

By comparing the AE signal characteristics of the rock under different upper-stress limit cyclic loads in Figure 4 with Figure 2, it could be found that under different cyclic static load upper-stress limits, the AE signal characteristics of the rock in the initial loading stage were consistent with the corresponding AE signal characteristics in the range of not greater than the upper-stress limit in Figure 2. In order to compare the characteristic changes of the AE signal during the cyclic loading and unloading process more intuitively, the cyclic loading and unloading were used to continue loading until it was broken, as shown in Figure 6.

It can be seen from the experimental results in Figure 6 that from the end of the first loading and unloading phase to the last loading and before the destruction, AE events accounted for 1.58% of the total number of AE events, which was negligible compared with the total number of AE during the entire experiment. Compared with the experimental results of the AE signal characteristics of the rock under uniaxial load in Figure 2, except for the middle cyclic loading and unloading phase, the characteristics of the AE signals in the two figures are consistent with the increase in stress. In addition, in the cyclic loading and unloading phase, when the stress did not exceed the maximum value in its stress history, there were almost few new



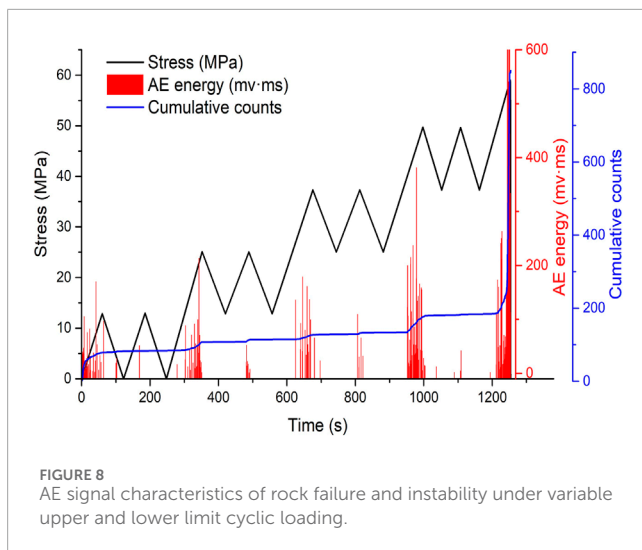
AE events in the rock. This result was also consistent with the results of the cyclic loading and unloading test in Figure 4.

By analyzing the experimental results of AE characteristics of rocks under equal upper and lower limit cyclic loads, it could be seen that the AE signal characteristics of rocks under low-frequency cyclic loading and unloading were related to the upper limit of cyclic static load stress. In addition, during the whole process of continuous loading and unloading of the rock after being cyclically loaded and unloaded by the low frequency and other upper and lower limits, the AE signal characteristics of the loaded rock under different stress levels were consistent with the AE signal characteristics of the rock under uniaxial load.

In order to analyze the AE signal characteristics of rock under cyclic loading more comprehensively. In addition to analyzing the AE characteristic test of rock under the action of fixed upper and lower limits cyclic load, the AE signal characteristic of rock under the action of variable upper and lower limit cyclic load should also be analyzed. Therefore, the next method is to change the upper and lower limits to analyze the characteristics of the AE signal of the rock under the cyclic load, as shown in Figure 7.

From the test results shown in Figure 7, it can be seen that the AE signal characteristics of the loaded rock are similar to those in Figure 5. The difference from the test result in Figure 5 is that the lower stress limit in Figure 7 is not 0 but the upper stress limit in the last cyclic loading stage. Due to the difference in the lower stress limit, in the cyclic loading and unloading process of each stress upper limit in Figure 7, except for the first loading stage, the AE events in the rest are less than those in Figure 5. This is because under the influence of the loading equipment, when the stress is low, the loading device is disturbed by the unstable oil pressure, so the difference between Figures 5, 7 appears. Therefore, in order to reduce the error caused by the unstable oil pressure, a cyclic load with fixed upper and lower limits is used to act on the rock specimen, and the load is continued until the rock is crushed and becomes unstable, as shown in Figure 8.

From the experimental results in Figure 8, the number of AE events emitted by the cyclic loading phase with distinct upper-stress limits could be seen intuitively. When the stress applied to the sandstone was greater than $0.8\sigma_b$, the AE events were the most



and the growth rate was the largest, and at the same time, the AE energy also reached the maximum. At this time, the cracks in the loaded rock increased exponentially until the rock was crushed and lost stability. Affected by changes in the internal physical structure of the rock, when the upper limit of the cyclic static load stress was less than $0.2 \sigma_b$, the primary pores in the rock under the load were compacted and closed and an AE event was emitted. The number of AE events was related to the internal structure of the rock. When the number of pores in the rock was large, the number of AE events was larger, and the larger the size of the primary pores, the greater the AE energy, and *vice versa*. Therefore, there were more AE events emitted by the loaded rock in this stage, but the AE energy was smaller. When the bearing stress of the loaded rock was greater than $0.2 \sigma_b$ and less than $0.6 \sigma_b$, the rock was in the elastic deformation stage, and the solid mineral particles mainly bear the rock deformation under the load. In addition, when a small number of solid mineral particles ruptured the cemented matrix under the influence of the tip effect and emitted an AE event, the AE energy released during this rupture was greater than the AE energy emitted when the primary pores were compacted and closed. Therefore, there were fewer AE events in this stage, and the AE energy was larger. When the load stress of the bearing rock exceeded $0.6 \sigma_b$ and was less than $0.8 \sigma_b$, the cemented matrix in the bearing rock began to crack gradually. At this time, there were more AE events and greater AE energy than the previous two stages. In summary, start loading from 0 and gradually increased with a gradient of $0.2 \sigma_b$ in the five loading ranges, when the loading stress was greater than $0.8 \sigma_b$, the cumulative count and growth rate of AE both reached the maximum, followed by the loading stress less than $0.2 \sigma_b$, and when the loading stress was $0.4 \sigma_b$ and $0.6 \sigma_b$, the two stages were the smallest.

The AE signal characteristics of the loaded rock in Figure 8, if it was regarded as the initial loading stage that only considered the cyclic load of each upper-stress limit, and connected them together until the rock was loaded and destroyed, the change rule of the AE signal characteristic during the whole process was consistent with Figure 2 of the loaded rock under uniaxial load. At the same time, the AE signal characteristics of the loaded rock under the

action of low-frequency cyclic loading and unloading were also verified.

4 Conclusion

1. The AE accumulative count of rock under uniaxial load gradually increases, and its growth rate increases rapidly in a short period of time, then approaches 0 and remains unchanged, and finally increases sharply. AE energy increases sequentially in these three stages, and the last stage increases sharply.
2. For rocks under low-frequency fixed-upper limit cyclic loading, the AE event mainly occurs in the loading part of the first loading and unloading stage. For rocks under low-frequency fixed upper and lower limits cyclic loading, when the loading stress is not greater than the maximum value in the stress history of the loaded rock, few new AE events are generated in the loaded rock.
3. After the low-frequency cyclic static load, the AE signal changes with the load-bearing stress of the rock during the whole process from continuous loading to failure, which is consistent with the characteristics of the AE signal of the loaded rock under uniaxial load.

Data availability statement

The original contributions presented in the study are included in the article/Supplementary material, further inquiries can be directed to the corresponding author.

Author contributions

QZ: Conceptualization, Data curation, Formal Analysis, Investigation, Methodology, Software, Validation, Writing—original draft. LZ: Conceptualization, Funding acquisition, Investigation, Methodology, Project administration, Resources, Supervision, Writing—review and editing. XJ: Data curation, Formal Analysis, Visualization, Writing—review and editing.

Funding

The author(s) declare that no financial support was received for the research, authorship, and/or publication of this article.

Conflict of interest

Authors LZ and XJ were employed by Cathay Safety Technology Co., Ltd.

The remaining authors declare that the research was conducted in the absence of any commercial or financial relationships that could be construed as a potential conflict of interest.

Publisher's note

All claims expressed in this article are solely those of the authors and do not necessarily represent those of their affiliated

organizations, or those of the publisher, the editors and the reviewers. Any product that may be evaluated in this article, or claim that may be made by its manufacturer, is not guaranteed or endorsed by the publisher.

References

- Borodii, M. V., and Adamchuk, M. P. (2010). Numerical simulation cyclic creep effect according to uniaxial loading programs. *Strength Mater* 42, 711–716. doi:10.1007/s11223-010-9258-5
- Chen, W., Li, S., Li, L., and Shao, M. (2020a). Strengthening effects of cyclic load on rock and concrete based on experimental study. *Int. J. Rock Mech. Min. Sci.* 135, 104479. Article number: 104479. doi:10.1016/j.ijrmms.2020.104479
- Chen, Y., Lin, H., Wang, Y., and Zhao, Y. (2020b). Damage statistical empirical model for fractured rock under freezing-thawing cycle and loading. *Geofluids* 2020, 1–12. Article ID: 8842471. doi:10.1155/2020/8842471
- Ferrero, A. M., Migliazza, M., and Tebaldi, G. (2010). Development of a new experimental apparatus for the study of the mechanical behaviour of a rock discontinuity under monotonic and cyclic loads. *Rock Mech. Rock Eng.* 43, 685–695. doi:10.1007/s00603-010-0111-8
- Ghasemi, S., Khamsehchiyan, M., Taheri, A., Nikudel, M. R., and Zalooli, A. (2021). Microcracking behavior of gabbro during monotonic and cyclic loading. *Rock Mech. Rock Eng.* 54, 2441–2463. doi:10.1007/s00603-021-02381-7
- Huang, D., Cen, D., Ma, G., and Huang, R. (2015). Step-path failure of rock slopes with intermittent joints. *Landslides* 12 (5), 911–926. doi:10.1007/s10346-014-0517-6
- Kan, Z., Zhang, L., Li, M., Yuan, X., and Huang, M. (2021). Investigation of seepage law in broken coal and rock mass under different loading and unloading cycles. *Geofluids* 2021, 1–14. Article ID: 8127250. doi:10.1155/2021/8127250
- Khaledi, K., Mahmoudi, E., Datcheva, M., and Schanz, T. (2016). Analysis of compressed air storage caverns in rock salt considering thermo-mechanical cyclic loading. *Environ. Earth Sci.* 75 (15), 1149. Article number: 1149. doi:10.1007/s12665-016-5970-1
- Li, N., Li, B., Chen, D., Wang, E., Tan, Y., Qian, J., et al. (2020a). Waveform characteristics of earthquakes induced by hydraulic fracturing and mining activities: comparison with those of natural earthquakes. *Nat. Resour. Res.* 29, 3653–3674. doi:10.1007/s11053-020-09699-z
- Li, Q., Liang, Y., Zou, Q., and Li, Q. (2020b). Acoustic emission and energy dissipation characteristics of gas-bearing coal samples under different cyclic loading paths. *Nat. Resour. Res.* 29, 1397–1412. doi:10.1007/s11053-019-09508-2
- Li, X., Wang, E., Li, Z., Liu, Z., Song, D., and Qiu, L. (2016). Rock burst monitoring by integrated microseismic and electromagnetic radiation methods. *Rock Mech. Rock Eng.* 49 (11), 4393–4406. doi:10.1007/s00603-016-1037-6
- Li, X., Wang, Y., Xu, S., Yang, H., and Li, B. (2021). Research on fracture and energy evolution of rock containing natural fractures under cyclic loading condition. *Geofluids* 2021, 1–13. Article number: 9980378. doi:10.1155/2021/9980378
- Liu, Q., Xu, J., Liu, X., Jiang, J., and Liu, B. (2015). The role of flaws on crack growth in rock-like material assessed by AE technique. *Int. J. Fract.* 193, 99–115. doi:10.1007/s10704-015-0021-6
- Liu, S., Li, X., Wang, D., Wu, M., Yin, G., and Li, M. (2020). Mechanical and acoustic emission characteristics of coal at temperature impact. *Nat. Resour. Res.* 29, 1755–1772. doi:10.1007/s11053-019-09562-w
- Liu, S., Li, X., Wang, D., and Zhang, D. (2021). Experimental study on temperature response of different ranks of coal to liquid nitrogen soaking. *Nat. Resour. Res.* 30, 1467–1480. doi:10.1007/s11053-020-09768-3
- Liu, X., Tan, Y., Ning, J., Tian, C., and Tian, Z. (2016). Energy criterion of abutment pressure induced strain-mode rockburst. *Rock Soil Mech.* 37 (10), 2929–2936. doi:10.16285/j.rsm.2016.10.026
- Liu, X. S., Tan, Y., Ning, J. G., and Gu, Q. H. (2016a). Damage constitutive model based on energy dissipation for intact rock subjected to cyclic loading. *Int. J. Rock Mech. Min. Sci.* 85, 27–32. doi:10.1016/j.ijrmms.2016.03.003
- Luo, Y., Gong, F., Li, X., and Wang, S. (2020). Experimental simulation investigation of influence of depth on spalling characteristics in circular hard rock tunnel. *J. Central South Univ.* 27 (3), 891–910. doi:10.11771-020-4339-5
- Ma, T., and Chen, P. (2014). Study of meso-damage characteristics of shale hydration based on CT scanning technology. *Petroleum Explor. Dev.* 41 (2), 249–256. doi:10.1016/S1876-3804(14)60029-X
- Marinelli, F., and Buscarnera, G. (2019). Anisotropic breakage mechanics: from stored energy to yielding in transversely isotropic granular rocks. *J. Mech. Phys. Solids* 129 (8), 1–18. doi:10.1016/j.jmps.2019.04.013
- Qian, J., Wang, K., Zhang, H., Tan, Y., Xu, C., Wang, Q., et al. (2022). First observation of paired microseismic signals during solution salt mining. *Front. Earth Sci.* 10, 952314. Article number: doi:10.3389/feart.2022.952314
- Qian, J., Zhang, H., and Westman, E. (2018). New time-lapse seismic tomographic scheme based on double-difference tomography and its application in monitoring temporal velocity variations caused by underground coal mining. *Geophys. J. Int.* 215, 2093–2104. doi:10.1093/gji/ggy404
- Qian, Q., and Zhou, X. (2018b). Failure behaviors and rock deformation during excavation of underground cavern group for jinping I hydropower station. *Rock Mech. Rock Eng.* 51, 2639–2651. doi:10.1007/s00603-018-1518-x
- Shi, H., Chen, W., Zhang, H., and Song, L. (2023a). A novel obtaining method and mesoscopic mechanism of pseudo-shear strength parameter evolution of sandstone. *Environ. Earth Sci.* 82, 60. Article number: 60. doi:10.1007/s12665-023-10748-y
- Shi, H., Chen, W., Zhang, H., Song, L., Li, M., Wang, M., et al. (2023b). Dynamic strength characteristics of fractured rock mass. *Eng. Fract. Mech.* 292, 109678. doi:10.1016/j.engfracmech.2023.109678
- Si, X., Luo, Y., and Luo, S. (2024). Influence of lithology and bedding orientation on failure behavior of “D” shaped tunnel. *Theor. Appl. Fract. Mech.* 129, 104219. Article number: 104219. doi:10.1016/j.tafmec.2023.104219
- Song, S., Liu, X., Tan, Y., Fan, D., Ma, Q., and Wang, H. (2020). Study on failure modes and energy evolution of coal-rock combination under cyclic loading. *Shock Vib.* 2020, 1–16. Article number: 5731721. doi:10.1155/2020/5731721
- Song, Z., Konietzky, H., and Herbst, M. (2019). Bonded-particle model-based simulation of artificial rock subjected to cyclic loading. *Acta Geotech.* 14 (4), 955–971. doi:10.1007/s11440-018-0723-9
- Sun, W., Wu, A., Hou, K., Yang, Y., and Wen, Y. (2016). Real-time observation of meso-fracture process in backfill body during mine subsidence using X-ray CT under uniaxial compressive conditions. *Constr. Build. Mater.* 113, 153–162. doi:10.1016/j.conbuildmat.2016.03.050
- Tan, Y. L., Zhao, T. B., and Xiao, Y. X. (2010). *In situ* investigations of failure zone of floor strata in mining close distance coal seams. *Int. J. Rock Mech. Min. Sci.* 47 (5), 865–870. doi:10.1016/j.ijrmms.2009.12.016
- Vaneghi, R. G., Ferdosi, B., Okoth, A. D., and Barnabas, K. (2018). Strength degradation of sandstone and granodiorite under uniaxial cyclic loading. *J. Rock Mech. Geotechnical Eng.* 10 (1), 117–126. doi:10.1016/j.jrmge.2017.09.005
- Wang, Y., Tang, J., Dai, Z., and Yi, T. (2018). Experimental study on mechanical properties and failure modes of low-strength rock samples containing different fissures under uniaxial compression. *Eng. Fract. Mech.* 197 (11), 1–20. doi:10.1016/j.engfracmech.2018.04.044
- Waples, D. W., and Waples, J. S. (2004). A review and evaluation of specific heat capacities of rocks, minerals, and subsurface fluids. Part 1: minerals and nonporous rocks. *Nat. Resour. Res.* 13, 97–122. doi:10.1023/B:NARR.0000032647.41046.e7
- Wei, P., Li, X., Hu, Q., Peng, S., and Liu, S. (2020). A trapezoidal three-dimensional model for gas extraction based on shapes of caved overlying strata and numerical calculation. *Nat. Resour. Res.* 29, 4031–4051. doi:10.1007/s11053-020-09677-5
- Wu, J., Wong, H., Zhang, H., Yin, Q., Jing, H., and Ma, D. (2024). Improvement of cemented rockfill by premixing low-alkalinity activator and fly ash for recycling gangue and partially replacing cement. *Cem. Concr. Compos.* 145, 105345. doi:10.1016/j.cemconcomp.2023.105345
- Wu, Y., Song, X., Ventura, C., and Lamd, F. (2020). Rocking effect on seismic response of a multi-story traditional timber pagoda model. *Eng. Struct.* 209, 110009. Article number: 110009. doi:10.1016/j.engstruct.2019.110009
- Xin, X., Lei, F., ZhiyuZhang, S. G., Zhang, S., Zhang, Y., and Yihu, Z. (2021). Blasting relaxation characteristics of columnar jointed rock mass with AE technology. *Arabian J. Geoscience* 14, 2827. Article number: 2827. doi:10.1007/s12517-021-08975-3
- Yang, S. Q., and Jing, H. W. (2011). Strength failure and crack coalescence behavior of brittle sandstone samples containing a single fissure under uniaxial compression. *Int. J. Fract.* 168, 227–250. doi:10.1007/s10704-010-9576-4
- Zheng, Q., Hu, H., Yuan, A., Li, M., Wang, H., Wang, M., et al. (2020). Impact dynamic properties and energy evolution of damaged sandstone based on cyclic loading threshold. *Shock Vib.* 2020, 1–12. Article number: 6615602. doi:10.1155/2020/6615602

Zheng, Q., Qian, J., Zhang, H., Chen, Y., and Zhang, S. (2024). Velocity tomography of cross-sectional damage evolution along rock longitudinal direction under uniaxial loading. *Tunn. Undergr. Space Technol.* 143, 105503. Article number: 105503. doi:10.1016/j.tust.2023.105503

Zheng, Q., Xu, Y., Hu, H., Qian, J., Ma, Y., and Gao, X. (2021). Quantitative damage, fracture mechanism and velocity structure tomography of sandstone under uniaxial load based on acoustic emission monitoring technology. *Constr. Build. Mater.* 272, 121911. Article number: 121911. doi:10.1016/j.conbuildmat.2020.121911

Zheng, Q., Xu, Y., Hu, H., Qian, J., Zong, Q., and Xie, P. (2021). Fracture and tomography of velocity structures of sandstone under uniaxial loads. *Chin. J. Geotechnical Eng.* 43 (6), 1173–1182. doi:10.11779/CJGE202106010

Zheng, Q., Cheng, Y. H., Zong, Q., Xu, Y., Li, F. H., and Chen, P. Y. (2019). Failure mechanism of different types of shotcrete based on modified Weibull distribution model. *Constr. Build. Mater.* 224, 306–316. doi:10.1016/j.conbuildmat.2019.07.071

Zhu, Z., Fang, Z., Xu, F., Han, Z., Guo, X., and Ma, C. (2022). Model test study on the rock mass deformation law of a soft rock tunnel under different ground stresses. *Front. Earth Sci.* 10. Article number: 962445. doi:10.3389/feart.2022.962445